electronics

Article

SC-FDE Layer for Sensor Networks in Remote Areas Using NVIS Communications

Tomas Gonzalez, Joaquim Porte, Jordi Male, Joan Navarro, Josep M. Maso, Agustín Zaballos, Joan L. Pijoan * and David Badia

La Salle Campus, Ramon Llull University, 08022 Barcelona, Spain; tomas.gonzalez@salle.url.edu (T.G.); joaquim.porte@salle.url.edu (J.P.); jordi.male@salle.url.edu (J.M.); jnavarro@salleurl.edu (J.N.); josep.maso@salle.url.edu (J.M.M.); agustin.zaballos@salle.url.edu (A.Z.); david.badia@salle.url.edu (D.B.)

* Correspondence: joanlluis.pijoan@salle.url.edu

Abstract: Despite high costs and lengthy deployments, satellite communications have traditionally been used to provide coverage in remote areas. However, given the fact that there is no radio infrastructure available in these areas, Near Vertical Incidence Skywave (NVIS) technology has positioned itself as an attractive alternative to communicate with low-power nodes in remote areas. This type of communication works in the HF frequency range complying with STANAG and MIL-STD standards, which define a physical layer for scenarios that differ from NVIS and low-power communication. The purpose of this paper was to present the definition of a new communication physical layer based on single-carrier frequency-domain equalization (SC-FDE) based on these standards but adapted to the ionospheric communication channel. This physical layer was compared to an OFDM-based layer from a previous study. The experiments performed show that this new approach achieves better results than OFDM in terms of a higher signal quality with a higher specific BER probability. Finally, this layer was also used in the theoretical design of an NVIS gateway to link sensor network devices spanning large-scale remote areas in a secure manner in the context of ubiquitous sensor networks (USN).

Keywords: remote sensing; HF; NVIS; IoT; OFDM; SC-FDE; SDR

Citation: Gonzalez, T.; Porte, J.; Male, J.; Navarro, J.; Maso, J.M.; Zaballos, A.; Pijoan, J.L.; Badia, D. SC-FDE Layer for Sensor Networks in Remote Areas Using NVIS Communications. *Electronics* **2021**, *10*, 1636. https://doi.org/10.3390/electronics10141636

Academic Editor: Davide Brunelli

Received: 12 June 2021
Accepted: 6 July 2021
Published: 9 July 2021

1. Introduction

The use of sensor networks in remote areas plays a fundamental role in the development of applications such as fire detection and human rescue, among others. Monitoring these difficult-to-access areas and collecting in-field data have emerged as a popular research topic in the last 20 years [1,2]. This has motivated the conception of new distributed-computing paradigms such as the Internet of Things (IoT) or Ubiquitous Sensor Networks (USN) [1], in which several devices are deployed in a certain scenario and link together by means of a wireless (or not) network. There are many wireless technologies currently in use for IoT sensors [3]. Most of them (such as LoRa or Sigfox) rely entirely on already deployed infrastructure, which complicates their deployment in under-resourced or difficult-to-access areas. The most common way to install these networks for these kind of use-cases is using satellite communications. The main drawbacks of using satellites are their high installation cost [4,5] and their dependence on the satellite's orbit, which sometimes makes coverage difficult due to loss of line of sight (LOS) or low signal-to-noise ratio (SNR).

A cheaper and faster-to-deploy alternative without the need for LOS is Near Vertical Incidence Skywave (NVIS) that can be used to link nodes from a distributed sensor network spanning large-scale areas [6]. The NVIS technique is a good solution for deploying networks in infrastructureless (or remote) areas or in places where natural catastrophes have occurred. NVIS benefits from ionospheric reflection by transmitting high frequency (HF) signals with an angle of incidence between 70° and 90°. The ionosphere allows HF signals to bounce back due to ionization on some of its own layers, creating a coverage zone of approximately 250 km (depending on many factors, such as the frequency or the time of day). Despite that, not all of the HF band can be used in a NVIS link [7] and the frequencies at which radio signals refract are between 3 MHz and 10 MHz [7]. Currently, NVIS nodes can be implemented on SDR platforms [8,9] and can achieve bit rates of up to thousands of bps (if higher data rates were needed, multiple antennas could be used to take advantage of the multipath effect or with multiple antennas using different channels [10,11]).

NVIS have to follow HF standards, which usually work with single carriers such as Quadrature Amplitude Modulation (QAM) or Phase-shift keying (PSK). These modulations require time-domain equalization to avoid multipath effects of the channel. Time-domain equalization is a computationally intensive implementation [12], which makes it unsuitable for low-cost platforms. Most current communications standards use the multicarrier scheme because of its adaptability and simple equalization [13]. These modulations have become widespread thanks to the exploitation of spectral bandwidth and the usage of mathematical expressions such as Fast Fourier Transform and the Inverse Fast Fourier Transform (FFT and IFFT) that optimize performance. For instance, Orthogonal Frequency-Domain Multiplexing (OFDM) was used in older versions of Wi-Fi [14]. Additionally, Orthogonal Frequency-Division Multiple Access (OFDMA) and Single-Carrier Frequency Division Multiple Access (SC-FDMA) are currently used for LTE and 5G in downlink (DL) and up-link (UL), respectively [15]. Indeed, recent studies confirm that such modulations could be used for resource-limited IoT devices [16–18].

Considering these modulations in the context of ionospheric communications, the study performed in [19] compared SC-FDE with OFDMA and SC-FDMA with ionospheric communications in an oblique way. In [20], an alternative solution with an OFDM transmission was proposed to avoid the complex equalization (OFDM requires frequency-domain equalization) for NVIS communications using the Zero Forcing (ZF) equalization method. The main drawback is that the subdivision of the bandwidth into subcarriers presents peaks in the envelope that cause a reduction in amplification capability.

The SC-FDE modulation has attracted significant interest in the field of research. In [21], a study of of SC-FDE synchronization technology in HF wireless communication using Minimum Mean Square Equalizer (MMSE) was proposed. In [22], an online Long Short-Term Memory (LSTM) estimator using HF Multiple-Input Multiple-Output (MIMO) SC-FDE systems was discussed. Furthermore, [23] proposed an efficient-channel parameters-estimation design for SC-FDE in HF wireless communications. This research endorsed the idea that SC-FDE can (1) be used for scenarios with challenging and noisy channels and (2) outperform OFDM in terms of power consumption by solving high Peak-to-average Power Ratio (PAPR) issues [24].

This paper defined a protocol for low-power NVIS communications that applies SC-FDE modulation to link nodes from wireless sensor networks deployed in remote areas. Compared with OFDM, SC-FDE improves the PAPR and reduces the complexity of transmitting nodes, as it is less sensitive to Inter-Block Interference (IBI) and Inter-Carrier Interference (ICI) caused by the multipath effect [25–27].

The outline of the paper is as follows. First, a background study and a summary of the theoretical concepts used in the protocol definition is provided in Section 2. Secondly, the use case is explained in Section 3 to contextualize and analyze the design of the system explained in Section 4 and the framework design is detailed and schematized in Section 4. Section 5 exhibits the tests results and, finally, Section 6 presents the conclusions.

2. Background Study

The following subsections outline the theoretical background regarding (1) the evolution of the HF communications, (2) NVIS history and current characteristics, and (3) the SC-FDE modulation to be analyzed.

2.1. HF Communications Evolution

HF communications started out as point-to-point and shortwave, and were mostly used by radio amateurs. Technical evolution and continuous research have led to these communications being used over long distances with several generations of advances. The first generation (1G) focused on narrowband systems with amplitude modulations for voice transmission with a 3 kHz channel (current standards as STANAG and MIL-STD keeps this channel bandwidth). Subsequently, attempts were made to improve performance with different modulations such as FSK, PSK, or QAM. The main drawback was the choice of frequency, as it was variant during the day. In the second generation (2G), microprocessors were introduced, and progress was made towards digital communications and signal processing. With this, point-to-multipoint communications were achieved. Finally, an interesting development was the Automatic Link Establishment (ALE), which allowed not to be in constant analysis of frequencies, but had a high cost of computing and very poor signal processing. The third generation (3G) improved the links, being faster and with a lower SNR. It also supported larger networks, and improved the efficiency of the entire network by separating channels for link establishment and traffic communications. The fourth generation (4G) already involves advances in artificial intelligence and broadband, and seeks the integration of systems with high data volumes and throughput [28,29].

2.2. NVIS

The use of NVIS communications dates back to the Vietnam War in the late 1960s. However, it is known that this type of communication had already been in use since 1939 at the advent of World War II, although not under this name. These communications were high-powered and were aimed primarily for voice transmission. In these systems, reference was already made to the use of antennas as horizontal dipoles to cover bands from 2 to 8 MHz with the objective of covering 24 h of operation due to the bouncing characteristics of the ionosphere using short waves [30]. In the overview of [31], a brief review of the history of NVIS is provided which starts with the discussion of the existence of the Hevyside layer by [32] as well as the Appleton and Builder experiment using the ionosphere as a refraction medium [33]. The reason for the use of these communications boils down to their rapid deployment and widespread supply.

The HF band has always been used for long distance communications with antennas at a low angle to the horizon. In this way, a coverage area of 250 km around the transmitter is produced. However, the link distance depends on the angle: the smaller the angle, the lower the Maximum Usable Frequency (MUF), mainly between 3 and 10 MHz [7]. Even so, the biggest disadvantage of this type of communication is the availability and behavior of the ionosphere due to the ionization of its own layers and solar activity. This implies that these communications will not be available during certain times at the same frequency. The use of multiband antennas can assure communication for an entire day. As an advantage, these communications are easy to install due to their antennas, they usually feature low-cost platforms, and they do not require the transmitter and receiver to have direct line of sight, allowing them to overcome large mountains, which makes them ideal for remote areas.

The antennas are usually wired and dipole types in order to optimize performance [7]. The horizontal dipole and the inverted Vee are the most frequently used antennas for NVIS, the latter being more interesting due to the need for a single mast [34].

To reduce the size of the antennas and to power the sensors with batteries, an efficient physical layer is required that can work with the lowest possible transmit powers and simple equalization.

2.3. SC-FDE

SC-FDE has the particularity of having the IFFT function in the receiver, which solves the main multicarrier modulation problems (high PAPR and low signal-to-noise ratio). The IFFT is performed at the receiver side together with the FFT [35]. This avoids the need for precise frequency synchronization and for a linear amplifier. In addition, it has advantages such as having almost constant envelope characteristics, being considered a single carrier, and using a simple equalization as it is performed in the frequency domain [26]. Furthermore, it also maintains some of the advantages such as the integration of Cyclic Prefix (CP), where the multipath effect produced by ionospheric transmissions can be avoided, thus making the transmission more robust. Considering the ionosphere channel results in [36], the CP can be variably designed to fit the channel, resulting in higher efficiency without the need for multiple symbols to avoid multipath.

Figure 1 displays a block diagram of the OFDM modulation and the IFFT position change for the SC-FDE implementation. Serial bits are converted to symbols (Mapping), taking into account the modulation order after the parallel conversion. After that, the Cyclic Prefix is added to then convert all the symbols to serial again for transmission purposes. On the receiver side, the CP is removed and the FFT algorithm is applied. Then, the equalization is performed to compensate for the channel effects. Finally, the IFFT is applied along with the serial to parallel conversion in order to obtain the array of bits.

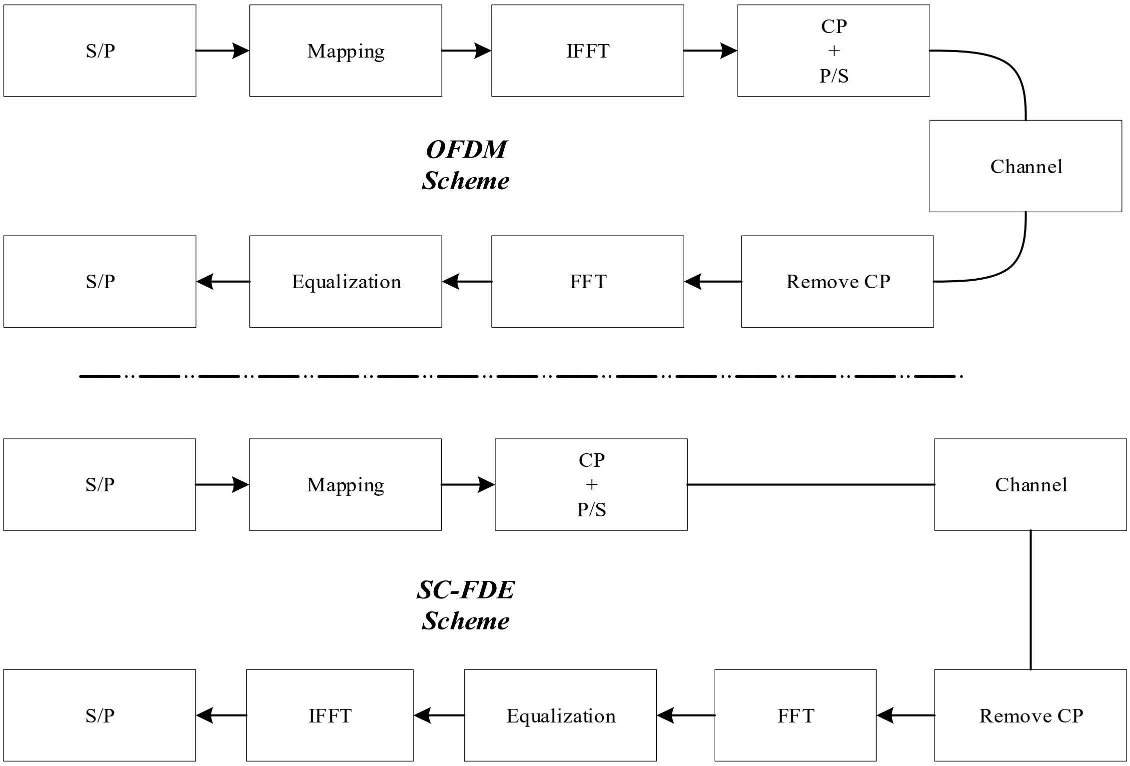

Figure 1. OFDM and SC-FDE schemes. Note the change of IFFT position between OFDM and SC-FDE.

In SC-FDE pilot schemes, values have a variation compared with other modulations. For example, OFDM can have a symbol full of pilots (all the subcarriers with the same value). In contrast, SC-FDE needs to have different pilot values due to the FFT, which converts these values to zero. Therefore, the root Zadoff-Chu sequence must be used, which is a sequence that presents different values but in-module are the same value [37].

SC-FDE modulation is noise-sensitive, so the equalization method can be improved by taking noise into account, as well as the effects of the channel.

Additionally, the study in [26] showed that other equalization types are better than the ZF. MMSE and Maximum Likelihood (ML) had the best performance. Nevertheless, the research performed in [38] showed that, despite being the one with the best results, the ML method is much more complex in computational terms. Therefore, it is also possible to estimate noise and use (1), which outperforms the (2) method when noise cannot be considered negligible, although it is not as robust against Inter-symbol Interference (ISI) [39]. H_{est} is the channel effect estimation and σ^2 is the variance of the noise.

$$H_{mmse} = \frac{H_{est}*}{(|H_{est}|^2 + \sigma^2)} \tag{1}$$

$$H_{zf} = \frac{1}{H_{est}} \tag{2}$$

As noted above, multicarrier techniques produce peaks due to the division of the channel into subcarriers, which produces a high PAPR value. Many techniques, such as the Crest Factor Reduction (CFR) try to reduce this negative point. This commonly used technique uses different methods to reduce the peaks such as Clipping and Filtering, Peak Windowing, and Peak Cancellation, among others. Clipping is a very good option to reduce the PAPR due to its low computational cost and high effectiveness [40,41]. It consists of saturating the signal above a fixed threshold called Clipping Ratio (CR). It helps to increase the average power; however, one of its main drawbacks is that it introduces higher nonlinearity, causing out-of-band emissions and interference to the target link.

The clipping ratio is calculated in Equation (3) and illustrated in Figure 2. It shows an example of how the signal reacts to this technique. The signal x(n) maintains its value as long as it does not exceed a certain threshold. This threshold is set from the maximum peak power. If x(n) overcomes the threshold the signal value automatically becomes the CR value (x_clipping(n) in the figure).

$$y(n) = \begin{cases} x(n), \ \max(|x(n)| < \ CR \\ CR, \ \max(|x(n)| \geq \ CR \end{cases} \tag{3}$$

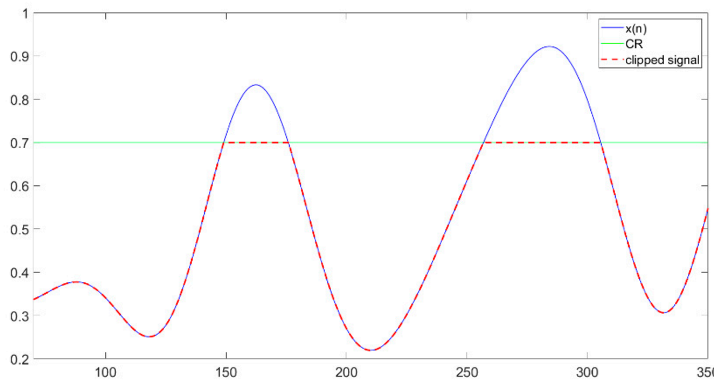

Figure 2. Clipping technique. The red line shows the original signal, and the blue line shows the clipped signal due to the threshold drawn in green [42].

3. Use Case

One of the great advantages of the NVIS technology is that it enables the rapid deployment of medium-distance (less than 250 km) communications with no line of sight at a very low cost. This results in a very convenient alternative when designing IoT environments for remote scenarios where sensing (and/or actuating) nodes are deployed to span large-scale areas and no other communication technologies are available.

In this case, as shown in Figure 3, the whole IoT scenario can best be viewed as a Ubiquitous Sensor Network [43] where sensors are grouped—by means of a concentrator/hub—around the NVIS node which, in turn, acts as a communication gateway to link with the nodes from neighboring IoT domains. In this way, the sensor network can use more standard communication technologies (e.g., Bluetooth, Wize) that are typically available in sensor devices. Additionally, following the principles of edge computing [44] and considering the limited bandwidth available at the NVIS link, this communication gateway can also behave as an edge node where data are aggregated and summarized. If an Internet connection were available at any IoT domain, the NVIS node could also behave as a sink node to forward all the collected data elsewhere.

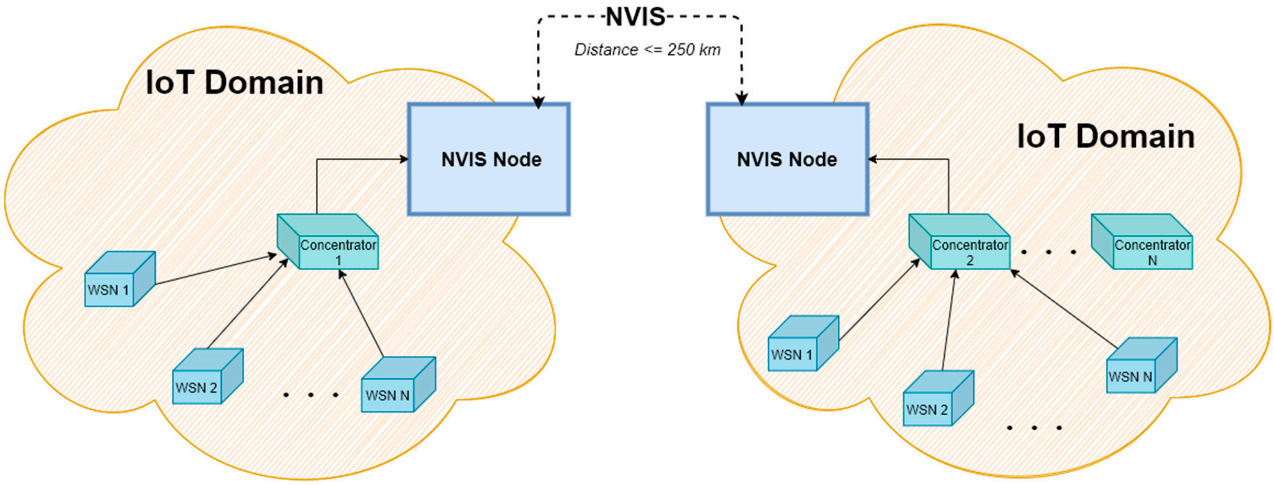

Figure 3. System model deployment.

4. System Design

In order to be able to establish a system adapted to the use case, we explain how the platform is composed and the design of the physical layer.

4.1. Platform Overview

The current platform is based on the concept of Software-Defined Sadio (SDR). SDR allows the independence of certain radio hardware components to operate independently as they are implemented by software. This fact offers many possibilities, especially when the transmitted protocols are not the same and some values (the carrier frequency, for example) need to be set several times for different scenarios.

The boards used for the signal processing were two Red Pitaya STEMLab 125-14 [45]. They present a ZYNQ SoC, including a field-programmable gate array (FPGA) and a central processing unit (CPU), an analog-digital converter (ADC) and a digital-analog converter (DAC). These converters present a resolution of 14 bits and are managed by a 125 MSPS clock.

The operating schemes of the Red Pitaya were based on two blocks: the processing system (PS) and the programmable logic (PL). On one side, the PS refers to the CPU, in which, in our case, an operating system (OS) is installed over this PS. This is where the configuration files are located and the peripherals, such as the external memory, are managed. On the other hand, the PL manages all the upsampling and downsampling, making use of the DUC/DDC converters that have been programmed using mainly FIR and CIC filters. The convergence of the two worlds is done through the RAM which, thanks to the direct shared memory (DMA), allows the transmission of data from the PS to the PL. In this case, the PS shares the data to be processed with the DMA, and the DMA passes the data to the PL through a FIFO memory where the DUC/DDC performs all the processing.

A microprocessor is connected to the Red Pitaya, which is in charge of time synchronization and the management of different peripherals. In addition, it is responsible for saving the raw files for transmission and also saving the received files for further post-processing. The microprocessor model chosen was the Raspberry Pi 3 [46].

A class-A amplifier was chosen to transmit signals with amplitude or phase changes that require linearity. The chosen model was a Bonn BLWA 0103-250 [47], which works at frequencies within the NVIS band and performs well in terms of efficiency. It was connected to the output of the Red Pitaya and enabled output powers above 54 dBm, although we should mention here that we did not use more than 25 W in our tests.

On the receiver side, an amplifier was used only to preamplify the signal by 30 dB without degrading its SNR. In addition, a Low Noise Amplifier (LNA) was used to perform proper demodulation. A Band Pass Filter (BPF) on both sides prevented external interference at frequencies around our carrier frequency. The carrier frequency was set to 5.4 MHz due to previous ionosphere behavior analysis. At the transmitter side, a horizontal dipole was used, and two inverted Vees were used at the receiver due to the straightforwardness of their installation, together with a respectable gain of 6.8 dB [48]. Having two antennas on the receiver increases the availability of communications by taking advantage of both the Ordinary and Extraordinary skywaves and using them to apply the Single Input Multiple Output (SIMO) technique, but in this case, we just used the Ordinary skywave due to its higher gain [49].

Figure 4 exhibits an overview of the whole system in a schematic way.

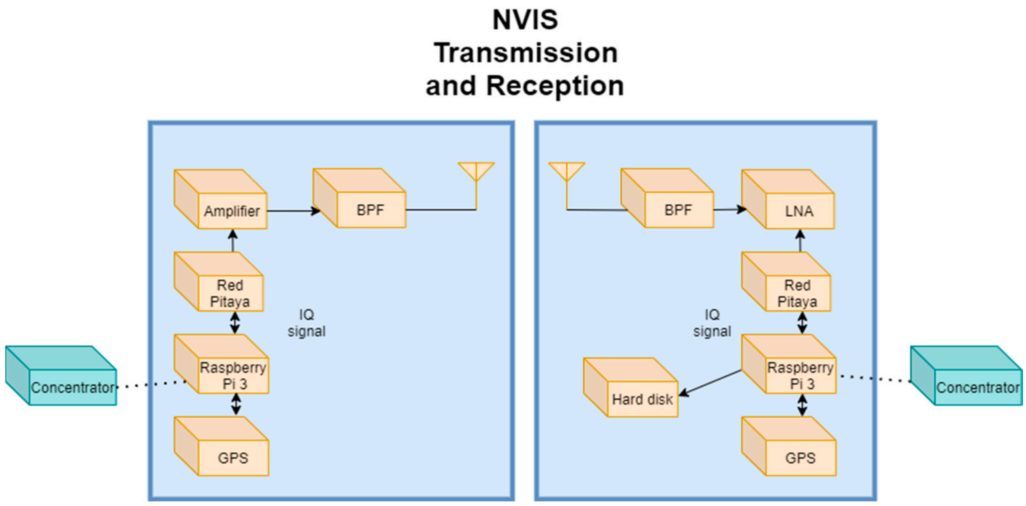

Figure 4. Near-vertical incidence skywave (NVIS) transmission scheme (transmitter on the left and receiver on the right).

4.2. Frame Design

In other NVIS studies, such as [8,9,49–51], narrowband modulations have proven that communications are quite reliable in a wide range of scenarios. So far, HF standards (military or otherwise) have used 3 kHz channels with single-carrier modulations such as PSK and QAM. An OFDM protocol was designed and tested in [47] for low-power applications with this same channel bandwidth.

The SC-FDE design follows almost the same structure as OFDM, only the SC-FDE concept distributes the symbols shorter in the time domain but longer in the frequency domain. The symbol length was calculated by simply dividing the symbol length defined in [20] by the number of subcarriers defined due to the coherence bandwidth. We kept the same CP due to the maximum delay spread of 3 ms. In fact, the study performed in [36] concluded that Delay Spread values for the Ordinary channel reached around 2.7 ms during the ionosphere availability. However, if we consider the mean, the values were about 0.5, so this fact caused the CP to have a very large error margin.

Finally, we used six SC-FDE symbols and only one extra symbol to obtain known sequences in order to have enough samples to perform an equalization. For our case, we chose the MMSE equalization, which is ideal for low SNR because it balances the channel and noise estimation.

With this configuration, a bit-rate of almost 4 kbps (2% more than the OFDM) and PAPR around 2 dB (more than 5 dB less than the OFDM) could be achieved, taking into account that it could have been even higher if the CP were variable and set to the mean Delay Spread (Ds) of the channel at a given time.

In Table 1, all the parameters of the SC-FDE design are summarized. Additionally, they are compared to the OFDM design proposed in [20] since they have a similar configuration.

Table 1. SC-FDE parameters.

Parameters	SC-FDE Values	OFDM Values
Bandwidth	3 kHz	3 kHz
Useful symbol length (TS)	0.33 ms	9.33 ms
Prefix cyclic length (TCP)	3 ms	3 ms
Number of subcarriers (NSC)	28	28
Number of symbols (Nsymbol)	7	7
Number of pilot/symbol	1	1
Number of data symbol	6	6
Packet duration	87.64 ms	86.31 ms
Bits in packet	336 bits	324 bits
Modulation	QPSK	QPSK
Equalization	MMSE	ZF
Bitrate of signal frame	3.833 kbps	3.753 kbps

5. Experimental Evaluation

In this section, we explain the tests that have been carried out to verify the behavior of the modulation depending on the power transmission considering the transmission success.

In this case, we wanted to evaluate a sweep of each Bit-error rate (BER) value and obtain its probability of occurrence. Moreover, to check how the channel and noise affect each modulation, many measures can be assessed, such as the Error Vector Magnitude (EVM), which measures the quality of the signals by looking at the deviation of the points from the ideal constellation due to the effects of the channel. Other alternatives include the Modulation Error Rate (MER), which is related to the EVM when average power is compared, or more commonly the BER-E_bN_0. In our research, we analyzed the BER-E_bN_0, a parameter that provides a quick overview of the received signal's performance.

For the tests, we decided to first check the success rate of the SC-FDE and decided to optimize the transmission power by adopting the clipping technique. In addition, we compared the BER/E_bN_0 with the OFDM, FSK, and QAM from the study performed in [20].

5.1. Test Area

The NVIS transmitter was located in La Salle Campus Barcelona (Spain). It has a horizontal dipole set at 5.4 MHz. The receiver, which consists of an inverted Vee, was located approximately 100 km away (Cambrils, Tarragona). Between these locations, there was no Line Of Sight (LOS) considering the elevation of the profile, which is more than 500 m high. The NVIS link is shown in Figure 5.

Figure 5. NVIS link between LaSalle Campus, BCN and Cambrils, Tarragona. The highest peak is located at 573 m above sea level.

5.2. Test Design

To test our system, a new protocol was defined following the same structure as in [20,48] but with the addition of the SC-FDE modulation. The frequency was fixed at 5.4 MHz.

A total of 50 frames were transmitted, each of which composed of a group of four packets. All frames started with an initial 6th Pseudorandom Noise (PN) sequence with re-sampling of 8 and having a length of 5 ms. This was used to do the packet synchronization.

Each packet was then composed by grouping a 60 ms tone, another 5 ms PN sequence, and one of the four modulations. The tone included in each packet allowed the Doppler shift of each modulation to be corrected. This effect is due to the Red Pitaya's clocks, which can provoke deviations of up to 10 Hz by side, so a total of 20 Hz of Doppler shift and the PN allows for the identification each modulation. Finally, this was repeated four times (once for each modulation) to form the frame.

IoT devices are usually remote, and battery usage requires low power consumption; therefore, transmission power must be minimized [52]. Knowing that the OFDM studied in [20] had sufficient performance around 12 W, our SC-FDE system was evaluated for 6, 12, and 25 W.

After this first approach, a second test rig was designed to perform the consumption optimization. A sweep of clipping values from 3 dB to 8 dB has been performed.

6. Results

This section presents the results achieved when comparing the transmission power to observe the cumulative distribution function (CDF) and OFDM along with the PAPR. The CDF graphs consist of different BER values on the abscissa axis (Xo in the figure) and the probabilities of obtaining them displayed at the ordinate axis (P(BER<Xo)).

6.1. BER CDF

Figure 6 exhibits a CDF graph of the BER computed in the received signals. It can be observed that having a peak power of 6 W, the probabilities of receiving a BER under 10^{-2} were remarkably high (more than 90%), but also a good performance to have a BER of 10^{-3}, which is over 70%. With regard to the 12 W test, the SC-FDE showed very good results, obtaining probabilities of over 80% for BER 10^{-3} and more than 90% for BER under 10^{-2}. Finally, for the same test with a peak power of 25 W, it can be observed that SC-FDE outperformed the other models, having probabilities of almost 90% to have BER 10^{-3} and around 95% for BER under 10^{-2}. As a first conclusion, it can be stated that the SC-FDE provides high yields for low power, especially around 12 W.

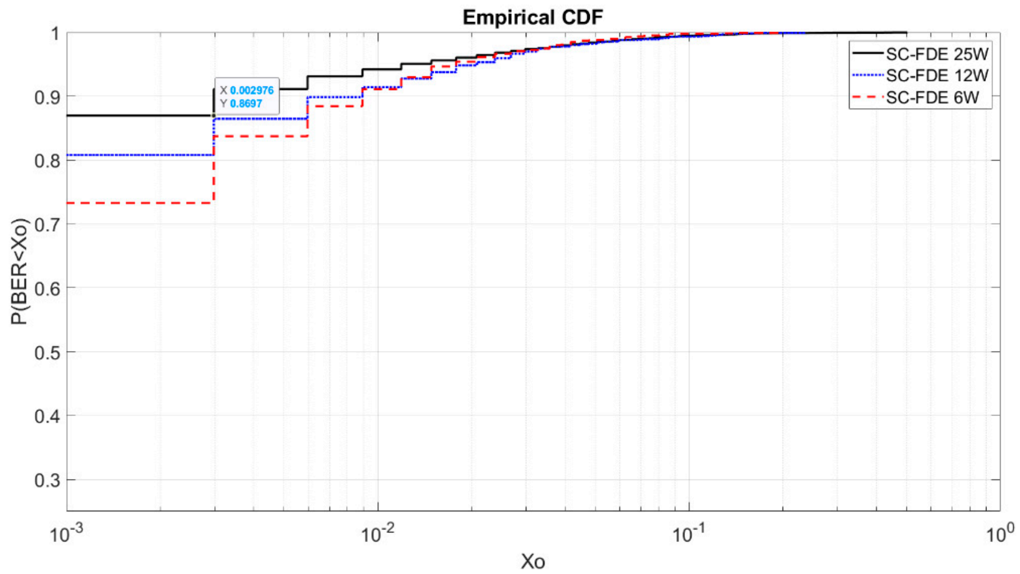

Figure 6. CDF plot of SC-FDE modulation with 6 W, 12 W, and 25 W of peak power.

6.2. BER vs. E_b/N_o

On the other hand, Figure 7 presents the relationship between received power (EbNo) and the BER obtained along with the FSK, QAM, and OFDM studied in [20].

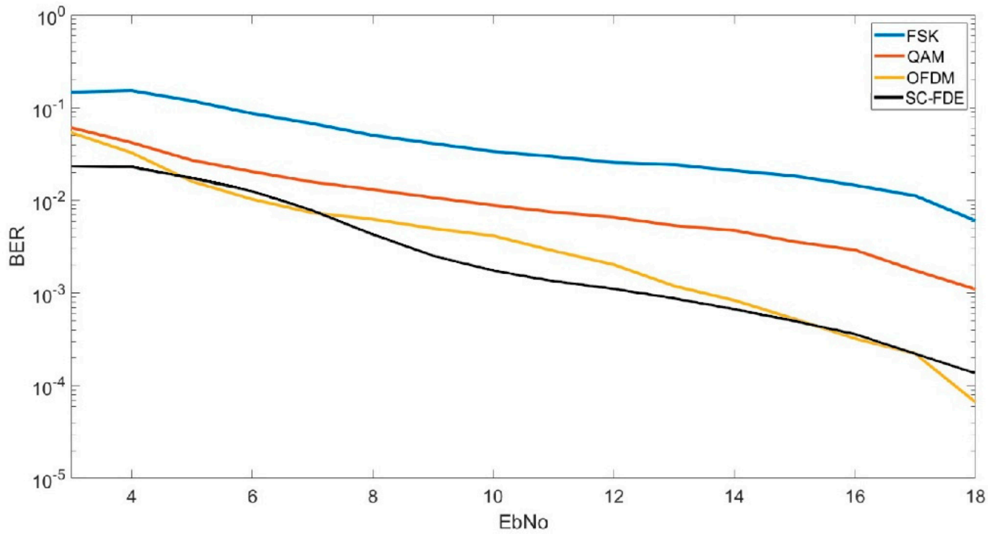

Figure 7. BER vs. EbNo comparison between FSK, QAM, OFDM, and SC-FDE.

FSK and QAM need higher EbNo than the OFDM and SC-FDE, which show very similar results. For BER of 10^{-3}, the SC-FDE needs 1 dB less than the OFDM, but for BER 10^{-4}, the OFDM needs 17.5 dB and the SC-FDE needs more than 18 dB.

6.3. CR Sweep

Taking into account these results and in a bid to raise the average power, a CR sweep was studied, with values starting at 3 dB with 1 dB steps up to 8 dBs. The higher the CR, the higher the Error Vector Magnitude (EVM) due to the saturation produced by the signal limitations. Despite having a higher EVM, the BER could be better due to the average power increase. The trade-off between power consumption and BER results must be considered.

As shown in Figure 8, we analyzed the CR tests with a transmitting power of 6 W. A significant difference can be observed when CRs were applied and when they were omitted. Initially, a probability of about 70% for a BER of 10^{-3} with a CR of 3 dB was obtained. If a CR of 6 dB was applied, a probability of more than 85% for a BER of 10^{-3} could be attained.

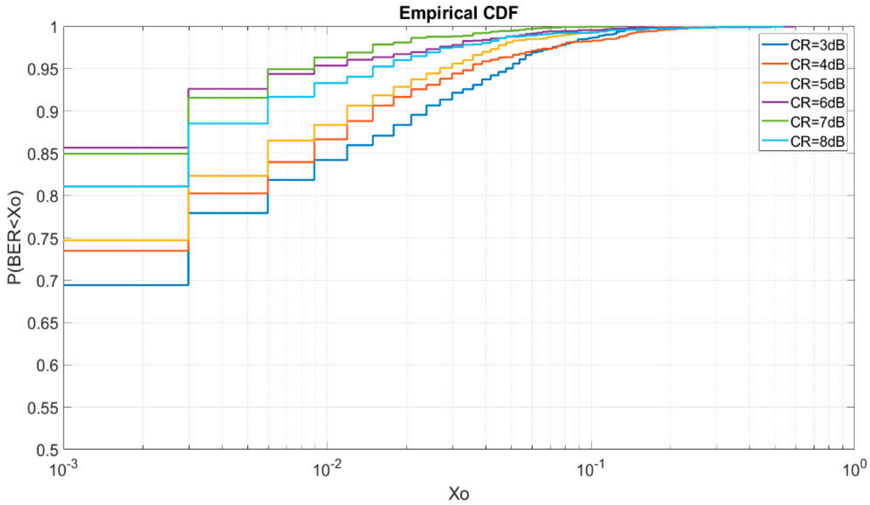

Figure 8. 6 W SC-FDE CR sweep CDF.

The graph below also shows how the CDF increases when the CR is higher. By dropping the peaks produced by the multicarrier splitting, the SNR and MER improved. However, from 6 dB (which is the best CR value) the CDF started to decrease again. This result was produced by the signal limiting, as the high-power peaks disappear and, therefore, relevant data was lost. This is the point where the EVM was large enough, and the increase of average power did not help due to the large in-band distortion.

6.4. CR Sweep 12 W

Figure 9 displays the same test of a peak power of 12 W. The results are quite similar, and only present some variations.

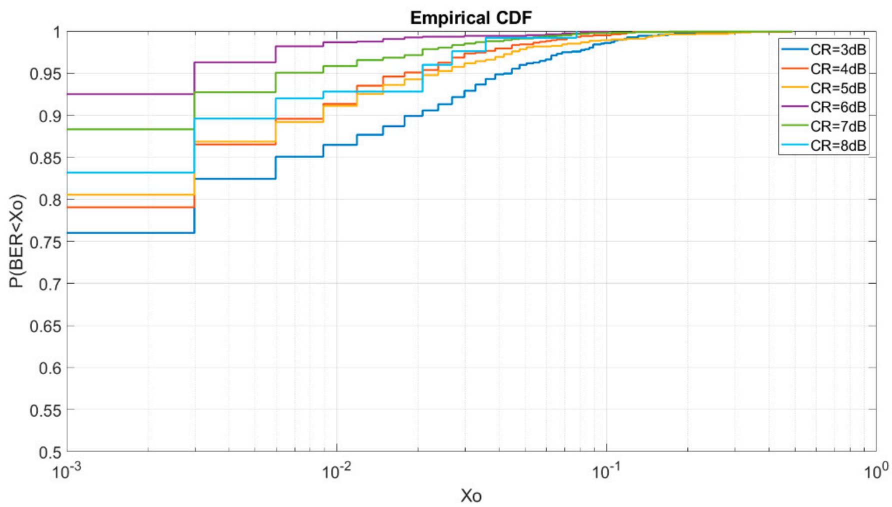

Figure 9. 12W SC-FDE CR sweep CDF.

6.5. CR Sweep 25 W

Figure 10 presents the results of the CR sweep for a peak power of 25 W. The point here is that the changes compared to 12 W were not that significant. For the low CR values, the increase of the performance was relevant. By contrast, the high values did not change so much.

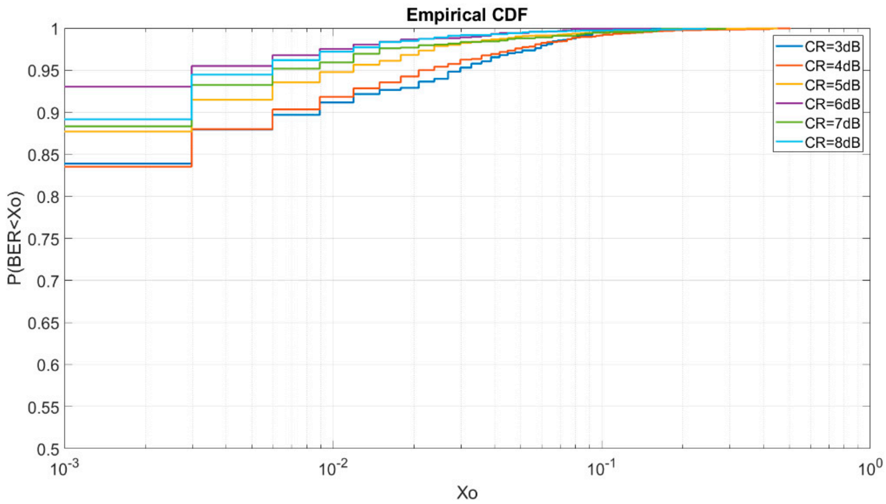

Figure 10. 25 W SC-FDE CR sweep CDF.

Results from Figure 10 show that 25 W is not worth implementing due to the higher consumption and near-identical behavior of 12 W. Comparing the three power scenarios, the BER-consumption ratio makes the 12 W the best configuration, saving the 6 W for more ideal scenarios without large multipaths or almost-null noise.

7. Conclusions

In this work we presented an analysis of the SC-FDE with the objective of improving the performance of NVIS communications following the STANAG and MIL-STD standards.

This study was carried out using two NVIS nodes 100 km apart. From the results of these transmissions, we can conclude that the SC-FDE together with an MMSE equalization obtains a much higher success rate than OFDM studied previously under the same conditions [20], making it much more efficient. As seen in the plots, this physical layer achieved a success rate of 93% BER 10^{-3} for the SC-FDE using the appropriate CR values at the expense of needing higher E_bN_0. With the same probability, the ODFM under the same conditions could only meet BER 10^{-2}. Apart from that, taking the best configuration of both, the OFDM needed a CR of 9 dB and the SC-FDE needed 3 dB less signal saturation. Moreover, by having the CP, the protection against the multipath effect is quite relevant. In addition, the CP set at the limits can be 33% more efficient in the case of no having multipath and slightly better if the symbol used to equalize has fewer pilot symbols. Finally, this physical layer will allow the use of low power amplifiers for battery-powered sensors, or use compact antennas with controlled losses of up to 10 dB. As an application, this protocol can be used as a platform for transmitting data collected from IoT devices and is suitable for USN thanks to the defined low transmitting powers. A disadvantage to take into account is that the bitrate in this type of communication is not particularly high, but it is not critical because remote sensors do not need high rates, but rather a strong communication robustness.

In future works, an exhaustive study of OFDM and SC-FDE together with their multiple access techniques (OFDMA and SC-FDMA) will be conducted, optimizing this physical layer, in order to try to define a complete uplink and downlink of NVIS technology. We will also study different bandwidths outside the standards in order to achieve higher bitrates.

Author Contributions: Investigation, T.G., J.P., J.M., J.L.P. and D.B.; methodology, J.L.P. and D.B.; software, T.G., J.P. and J.M.; supervision, A.Z., J.M.M., J.N., J.L.P. and D.B.; validation, J.L.P. and D.B.;

writing—original draft, T.G., J.P. and J.M.; writing—review & editing, T.G., J.P., J.M., J.N., J.M.M., A.Z., J.L.P. and D.B. All authors have read and agreed to the published version of the manuscript.

Funding: This research was funded by the Spanish Ministry on Science, Innovation and University, the Investigation State Agency and the European Regional Development Fund (ERDF) under the grant number RTI2018-097066-B-I00 (MCIU/AEI/FEDER, UE) for the project "NVIS SENSOR NETWORK FOR THE SOUTH SHETLAND ISLANDS ARCHIPELAGO" (SHETLAND-NET). This work received funding from the "Agència de Gestió d'Ajuts Universitaris i de Recerca (AGAUR)" of "Generalitat de Catalunya" (grant identification "2017 SGR 977").

Conflicts of Interest: The authors declare no conflict of interest.

Abbreviations

ADC	Analog-Digital Converter
BER	Bit-error rate
BPF	A Band Pass Filter
CDF	Cumulative Distribution Function
CFR	Crest Factor Reduction
CP	Cyclic Prefix
CPU	Central Processing Unit
CR	Clipping Ratio
DAC	Digital-Analog Converter
DL	Downlink
Ds	Delay Spread
EVM	Error Vector Magnitude
FFT	Fast Fourier Transform
FPGA	Field-programmable gate array
HF	High Frequency
IBI	Inter-Block Interference
ICI	Inter-Carrier Interference
IFFT	Inverse Fast Fourier Transform
IoT	Internet of Things
ISI	Inter-symbol Interference
LNA	Low Noise Amplifier
LOS	Line of Sight
LSTM	Long Short-Term Memory
LTE	Long-Term Evolution
MER	Modulation Error Rate
MIMO	Multiple Input Multiple Output
ML	Maximum Likelihood
MMSE	Minimum Mean Square Equalizer
MUF	Maximum Usable Frequency
NVIS	Near Vertical Incidence Skywave
OFDM	Orthogonal Frequency Division Multiplexing
OFDMA	Orthogonal Frequency-Division Multiple Access
PAPR	Peak-to-average Power Ratio
PN	Pseudorandom Noise
PSK	Phase-shift keying
QAM	Quadrature Amplitude Modulation
SC-FDE	Single-Carrier Frequency-domain Equalization
SC-FDMA	Single-Carrier Frequency Division Multiple Access
SDR	Software Defined Radio
SIMO	Single Input Multiple Output
SNR	Signal-to-noise ratio
UL	Uplink
USN	Ubiquitous Sensor Networks
USN	Ubiquitous Sensor Network
ZF	Zero Forcing

References

1. Bagula, A.; Zennaro, M.; Inggs, G.; Scott, S.; Gascon, D. Ubiquitous sensor networking for development (USN4D): An application to pollution monitoring. *Sensors* **2012**, *12*, 391–414. [CrossRef]
2. Wang, J.; Lim, M.K.; Wang, C.; Tseng, M.L. The evolution of the Internet of Things (IoT) over the past 20 years. *Comput. Ind. Eng.* **2021**, *155*, 107174. [CrossRef]
3. Gazis, V.; Gortz, M.; Huber, M.; Leonardi, A.; Mathioudakis, K.; Wiesmaier, A.; Zeiger, F.; Vasilomanolakis, E. A survey of technologies for the internet of things. In Proceedings of the IWCMC 2015—11th International Wireless Communications and Mobile Computing Conference, Dubrovnik, Croatia, 24–28 August 2015; Institute of Electrical and Electronics Engineers Inc.: Piscataway, NJ, USA, 2015; pp. 1090–1095. [CrossRef]
4. Smallsat Launch Services Feel Pricing Pressure-SpaceNews. Available online: https://spacenews.com/smallsat-launch-services-feel-pricing-pressure/ (accessed on 20 May 2021).
5. The Cost of Building and Launching a Satellite | Globalcom Satellite Phones. Available online: https://globalcomsatphone.com/costs/ (accessed on 20 May 2021).
6. Porte, J.; Briones, A.; Maso, J.M.; Pares, C.; Zaballos, A.; Pijoan, J.L. Heterogeneous wireless IoT architecture for natural disaster monitorization. *Eurasip J. Wirel. Commun. Netw.* **2020**, *2020*, 184. [CrossRef]
7. Witvliet, B.A.; van Maanen, E.; Petersen, G.J.; Westenberg, A.J.; Bentum, M.J.; Slump, C.H.; Schiphorst, R. Near Vertical Incidence Skywave Propagation: Elevation Angles and Optimum Antenna Height for Horizontal Dipole Antennas. *IEEE Antennas Propag. Mag.* **2015**, *57*, 129–146. [CrossRef]
8. Porte, J.; Maso, J.; Pijoan, J.L.; Miret, M.; Badia, D.; Jayasinghe, J. Education and e-health for developing countries using NVIS communications. In Proceedings of the IEEE Region 10 Humanitarian Technology Conference, R10-HTC, Malambe, Sri Lanka, 6–8 December 2019; Institute of Electrical and Electronics Engineers Inc.: Piscataway, NJ, USA, 2019. [CrossRef]
9. Porte, J.; Maso, J.; Pijoan, J.L.; Badia, D. Design, implementation, and test of an SDR for NVIS communications. *Int. J. Circuit Theory Appl.* **2019**, *47*, 1502–1512. [CrossRef]
10. Daniels, R.C.; Peters, S.W. A new MIMO HF data link: Designing for high data rates and backwards compatibility. In Proceedings of the Proceedings-IEEE Military Communications Conference MILCOM, San Diego, CA, USA, 18–20 November 2013; pp. 1256–1261. [CrossRef]
11. Daniels, R.C.; Peters, S.W.; Heath, R.W. HF MIMO NVIS measurements with co-located dipoles for future tactical communications. In Proceedings of the IEEE Military Communications Conference MILCOM, San Diego, CA, USA, 18–20 November 2013; pp. 1250–1255. [CrossRef]
12. Kuschnerov, M.; Piyawanno, K.; De Man, E.; Chouayakh, M.; Spinnler, B.; Alfiad, M.; Napoli, A.; Lankl, B. Data-aided single-carrier coherent receivers. In Proceedings of the Conference Proceedings-Lasers and Electro-Optics Society Annual Meeting-LEOS, Belek-Antalya, Turkey, 4–8 October 2009; pp. 638–639. [CrossRef]
13. Fazel, K.; Kaiser, S. Multi-Carrier and Spread Spectrum Systems: From OFDM and MC-CDMA to LTE and WiMAX | Wiley eBooks | IEEE Xplore. Available online: https://ieeexplore.ieee.org/book/8039579 (accessed on 29 April 2021).
14. Narasimhamurthy, A.B.; Banavar, M.K.; Tepedelenlioglu, C. OFDM Systems for Wireless Communications. *Synth. Lect. Algorithms Softw. Eng.* **2010**, *2*, 1–78. [CrossRef]
15. Navita, A.; Amandeep, N. Performance analysis of OFDMA, MIMO and SC-FDMA technology in 4G LTE networks. In Proceedings of the 2016 6th International Conference-Cloud System and Big Data Engineering, Confluence 2016, Noida, India, 14–15 January 2016; Institute of Electrical and Electronics Engineers Inc.: Piscataway, NJ, USA, 2016; pp. 554–558. [CrossRef]
16. Choi, J. Single-Carrier Index Modulation for IoT Uplink. *IEEE J. Sel. Top. Signal. Process.* **2019**, *13*, 1237–1248. [CrossRef]
17. Iraqi, Y.; Al-Dweik, A. Efficient Information Transmission Using Smart OFDM for IoT Applications. *IEEE Internet Things J.* **2020**, *7*, 8397–8409. [CrossRef]
18. Hussein, A.; Elgala, H. *Lightweight Multi-Carrier Modulation for IoT*; Broadband Access Communication Technologies XII; International Society for Optics and Photonics: San Francisco, CA, USA, 2018; p. 105590W. [CrossRef]
19. Hervás, M.; Alsina-Pagès, R.M.; Pijoan, J.L.; Salvador, M.; Badia, D. Advanced modulation schemes for an Antarctic Long Haul HF Link: Performance comparison between SC-FDE, OFDMA and SC-FDMA in a hostile environment. *Telecommun. Syst.* **2016**, *62*, 757–770. [CrossRef]
20. Maso, J.M.; Gonzalez, T.; Male, J.; Porte, J.; Pijoan, J.L.; Badia, D. NVIS multicarrier modulations for remote-sensor applications. *Sensors* **2020**, *20*, 6232. [CrossRef] [PubMed]
21. Boyuan, X.; Weizhang, X. Research of the SC-FDE synchronization technology in HF wireless communication. In Proceedings of the 2013 IEEE 8th Conference on Industrial Electronics and Applications, ICIEA 2013, Melbourne, Australia, 19–21 June 2013; pp. 1420–1423. [CrossRef]
22. Wang, Z.; Pu, F.; Yang, X.; Chen, N.; Shuai, Y.; Yang, R. Online LSTM-Based Channel Estimation for HF MIMO SC-FDE System. *IEEE Access* **2020**, *8*, 131005–131020. [CrossRef]
23. Duan, H.; Yu, X.; Hou, Y. Efficient channel parameters estimation design for SC-FDE in HF wireless communications. In Proceedings of the 2015 8th International Congress on Image and Signal Processing, CISP 2015, Shenyang, China, 14–16 October 2015; Institute of Electrical and Electronics Engineers Inc.: Piscataway, NJ, USA, 2015; pp. 1338–1342. [CrossRef]
24. Myung, H.G. Introduction to Single Carrier FDMA-IEEE Conference Publication. Available online: https://ieeexplore.ieee.org/document/7099187 (accessed on 22 April 2021).

25. Yoshizawa, S.; Tanimoto, H.; Saito, T. SC-FDE vs. OFDM: Performance comparison in shallow-sea underwater acoustic communication. In Proceedings of the 2016 International Symposium on Intelligent Signal Processing and Communication Systems, ISPACS 2016, Phuket, Thailand, 24–27 October 2016; Institute of Electrical and Electronics Engineers Inc.: Piscataway, NJ, USA, 2016. [CrossRef]
26. Pancaldi, F.; Vitetta, G.M.; Kalbasi, R.; Al-Dhahir, N.; Uysal, M.; Mheidat, H. Single-Carrier Frequency Domain Equalization [A focus on wireless applications]. *IEEE Signal Process. Mag.* **2008**. [CrossRef]
27. Si, L.; Yu, X.; Yin, H.; Xu, W. Compressive sensing-based channel estimation for SC-FDE system. *Eurasip J. Wirel. Commun. Netw.* **2019**, *2019*, 16. [CrossRef]
28. Wang, J.; Ding, G.; Wang, H. HF communications: Past, present, and future. *China Commun.* **2018**, *15*, 1–9. [CrossRef]
29. Johnson, E.E. *Third-Generation and Wideband HF Radio Communications*; Artech House: Norwood, MA, USA, 2013.
30. Austin, B.A. Near vertical incidence skywaves in World War II: An historical perspective. In Proceedings of the 8th International Conference on High-Frequency Radio Systems and Techniques, Guildford, UK, 10–13 July 2000; IET: Piscataway, NJ, USA, 2000; pp. 225–229. [CrossRef]
31. Witvliet, B.A.; Alsina-Pagès, R.M. Radio communication via Near Vertical Incidence Skywave propagation: An overview. *Telecommun. Syst.* **2017**, *66*, 295–309. [CrossRef]
32. Appleton, E.V.; Barnett, M.A.F. On some direct evidence for downward atmospheric reflection of electric rays. *Proc. R. Soc. Lond. Ser. Contain. Pap. Math. Phys. Character* **1925**, *109*, 621–641. [CrossRef]
33. Appleton, E.V.; Builder, G. The ionosphere as a doubly-refracting medium. *Proc. Phys. Soc.* **1933**, *45*, 208–220. [CrossRef]
34. Witvliet, B.A. Near Vertical Incidence Skywave: Interaction of Antenna and Propagation Mechanism. Available online: https://www.researchgate.net/publication/284284255_Near_Vertical_Incidence_Skywave_-_Interaction_of_Antenna_and_Propagation_Mechanism_PhD_Thesis (accessed on 20 May 2021).
35. Gomes, R.; Al-Daher, Z.; Hammoudeh, A.; Sobaihi, K.; Caldeirinha, R.; Fernandes, T. Performance and evaluation of OFDM and SC-FDE over an AWGN propagation channel under RF impairments using simulink at 60 GHz. In Proceedings of the 2014 Loughborough Antennas and Propagation Conference, LAPC 2014, Loughborough, UK, 10–11 November 2014; Institute of Electrical and Electronics Engineers Inc.: Piscataway, NJ, USA, 2014; pp. 685–689. [CrossRef]
36. Male, J.; Porte, J.; Gonzalez, T.; Maso, J.M.; Pijoan, J.L.; Badia, D. Analysis of the Ordinary and Extraordinary Ionospheric Modes for NVIS Digital Communications Channels. *Sensors* **2021**, *21*, 2210. [CrossRef]
37. De Figueiredo, F.A.P.; Mathilde, F.S.; Cardoso, F.A.C.M.; Vilela, R.M.; Miranda, J.P. Efficient frequency domain zadoff-chu generator with application to LTE and LTE-A systems. In Proceedings of the 2014 International Telecommunications Symposium, ITS 2014-Proceedings, Sao Paulo, Brazil, 17–20 August 2014; Institute of Electrical and Electronics Engineers Inc.: Piscataway, NJ, USA, 2014. [CrossRef]
38. Trimeche, A.; Sakly, A.; Mtibaa, A. FPGA Implementation of ML, ZF and MMSE Equalizers for MIMO Systems. *Procedia Comput. Sci.* **2015**, *73*. [CrossRef]
39. Hervás, M.; Pijoan, J.L.; Alsina-Pagès, E.M.; Salvador, M.; Badia, D. Single-carrier frequency domain equalisation proposal for very long haul HF radio links. *Electron. Lett.* **2014**, *50*, 1252–1254. [CrossRef]
40. Kim, W.J.; Cho, K.J.; Stapleton, S.P.; Kim, J.H. An efficient crest factor reduction technique for wideband applications. *Analog Integr. Circuits Signal. Process.* **2007**, *51*, 19–26. [CrossRef]
41. Ojima, M.; Hattori, T. PAPR reduction method using clipping and peak-windowing in CI/OFDM system. In Proceedings of the IEEE Vehicular Technology Conference, Baltimore, MD, USA, 30 September–3 October 2007; pp. 1356–1360. [CrossRef]
42. Crest Factor Reduction-RFmx SpecAn 19.1 Help-National Instruments. Available online: https://zone.ni.com/reference/en-XX/help/374264N-01/rfmxspecan/crest_factor_reduction/ (accessed on 19 April 2021).
43. Watch, T. Ubiquitous Sensor Networks (USN) ITU-T Technology Watch Briefing Report Series, No. 4. 2008. Available online: http://www.itu.int/md/T05-NGN.GSI-DOC-0266/en (accessed on 18 May 2021).
44. Yu, W.; Liang, F.; He, X.; Hatcher, W.G.; Lu, C.; Lin, J.; Yang, X. A Survey on the Edge Computing for the Internet of Things. *IEEE Access* **2017**, *6*, 6900–6919. [CrossRef]
45. Red Pitaya-Stemlab Swiss Army Knife for Engineers. Available online: https://www.redpitaya.com/ (accessed on 20 May 2021).
46. Raspberry Pi 3 Model B+–Raspberry Pi. Available online: https://www.raspberrypi.org/products/raspberry-pi-3-model-b-plus/ (accessed on 13 April 2021).
47. Bonn, E. Bonn Elektronik BLWA 0103-250 1.5.30 MHZ. Available online: http://frontend.bonn-elektronik.com/pdfsheet.php?modellreihe=140&smid=354&lang=eng (accessed on 2 June 2021).
48. Maso, J.M.; Porte, J.; Pijoan, J.L.; Badia, D. Study of NVIS channel for USN protocol definition in antarctica. *Electronics* **2020**, *9*, 1037. [CrossRef]
49. Maso, J.M.; Male, J.; Porte, J.; Pijoan, J.L.; Badia, D. Ionospheric polarization techniques for robust NVIS remote sensing platforms. *Appl. Sci.* **2020**, *10*, 3730. [CrossRef]
50. Maso, J.M.; Porte, J.; Pijoan, J.L.; Badia, D. Internet of Things Communications for Remote Sensors in Antarctica Using NVIS. 2019. Available online: https://www.researchgate.net/publication/335774336_Internet_of_things_communications_for_remote_sensors_in_Antarctica_using_NVIS (accessed on 20 April 2021).

51. Porté, J.; Lluis Pijoan, J.; Masó, J.; Badia, D.; Zaballos, A.; Maria Alsina-Pagès, R. Advanced HF Communications for Remote Sensors in Antarctica. In *Antarctica—A Key to Global Change*; IntechOpen: London, UK, 2018.
52. Nikoukar, A.; Raza, S.; Poole, A.; Gunes, M.; Dezfouli, B. Low-power wireless for the internet of things: Standards and applications. *IEEE Access* **2018**, *6*, 67893–67926. [CrossRef]